mathematics

MDPI

Article

Micropolar Dusty Fluid: Coriolis Force Effects on Dynamics of MHD Rotating Fluid When Lorentz Force Is Significant

Quanfu Lou [1], Bagh Ali [2], Saif Ur Rehman [3], Danial Habib [4], Sohaib Abdal [4], Nehad Ali Shah [5] and Jae Dong Chung [5,*]

[1] College of Education, Nanchang Normal College of Applied Technology, Nanchang 330108, China; hhu2000@163.com
[2] Faculty of Computer Science and Information Technology, Superior University, Lahore 54000, Pakistan; baghalisewag@gmail.com
[3] Department of Mathematics, University of Management and Technology, Lahore 54770, Pakistan; saifurrehman8684@gmail.com
[4] Department of Mathematics, Khwaja Fareed University of Engineering and Information Technology, Rheem Yar Khan 64200, Pakistan; danisheikh4006@gmail.com (D.H.); sohaibabdal8@gmail.com (S.A.)
[5] Department of Mechanical Engineering, Sejong University, Seoul 05006, Korea; nehadali199@yahoo.com
* Correspondence: jdchung@sejong.ac.kr

Abstract: The main objective of this investigation to examine the momentum and thermal transportation of rotating dusty micropolar fluid flux with suspension of conducting dust particles across the stretched sheet. The novelty of the flow model is the exploration of the significance of boosting the volume concentration of dust particles in fluid dynamics. The governing PDEs of the problem for both phase models are transmuted into nonlinear coupled non-dimensional ODEs by utilizing suitable similarity modifications. The bvp4c technique was utilized in MATLAB script to acquire a graphical representation of the experimental results. This study illustrates the analysis of repercussions of pertinent parameters on non-Newtonian fluid and the dusty phase of fluid. By improving the volume concentration of dust particles and rotating parameters, the axial velocity for both phases depreciates, whereas temperature and transverse velocity for both phases have the opposite behavior. The micro-rotation distribution rises with higher contributions of rotating and material parameters, whereas it decreases against larger inputs of volume concentration of dust particles. The growing strength of the dust volume fraction (ϕ_d) caused the coefficient of skin friction to decrease along the x direction, and the skin friction coefficient is raised along the y direction.

Keywords: dusty micropolar fluid; non-Newtonian fluid; rotational flow

MSC: 76D05; 76W05; 76-10

Citation: Lou, Q.; Ali, B.; Rehman, S.U.; Habib, D.; Abdal, S.; Shah, N.A.; Chung, J.D. Micropolar Dusty Fluid: Coriolis Force Effects on Dynamics of MHD Rotating Fluid When Lorentz Force Is Significant. *Mathematics* **2022**, *10*, 2630. https://doi.org/10.3390/math10152630

Academic Editors: Shujin Laima, Yong Cao, Xiaowei Jin and Hehe Ren

Received: 4 July 2022
Accepted: 25 July 2022
Published: 27 July 2022

1. Introduction

Eringen [1,2] proposed the theory of micropolar liquids, which is capable of explaining such fluids. The incorporation of novel kinematic variables is an important element to note in the development of Eringen's micro-continuum mechanics, such as the addition of the concept of body moments, gyration tensor, micro-inertia moment tensor, stress moments, and micro-stress averages to classical continuum mechanics. Nevertheless, substantial difficulties arise when this idea is implemented to real problems related to nontrivial flow; particularly in the case of linear theory, an issue involving basic micro-fluids must be expressed as a system of 19 PDEs with 19 unknowns. Moreover, the fundamental mathematical problem is challenging to solve. These unique characteristics for micropolar liquids were addressed in a comprehensive review of the subject and implications of micropolar liquid mechanics by Ariman et al. [3,4]. Early research in this area can be found in the review of [5], as well as in the more recent books, see [6,7]. Numerous investigators

considered the non-Newtonian fluid due to wide scope of real life applications [8,9]; liquid-containing tiny particles are the most important variables in heat conduction processes in fluids [10,11]. Solid particle incorporation in the base fluid impacts the dynamics of the fluid and can influence the fluids' efficient thermal conductivity [11,12]. According to Ali et al. [13], MHD could have a noteworthy impact on the improvement of thermal conductivity of non-Newtonian fluids. More work on non-Newtonian fluid subject to various types of geometries and Lorentz force was carried out in [14–17].

Although classical Newtonian liquids cannot accurately represent the features of fluid flow with suspended particles, the concept of micropolar liquids has received significant attention in recent years due to their potential in a variety of industrial processes [18,19]. Extrusion of polymer liquids, cooling of a metallic surface in a bath, crystal, animal blood, solidification of liquid, colloidal, suspension solutions, and novel lubricants are a few examples of micropolar liquid use. The essence of the concept of a micropolar liquid flow lies in the extension of constitutive equations for Newtonian liquids, which allow this theory to represent more complicated fluids [20]. According to this idea, rigid elements trapped in a small fluid volume element can only rotate around the volume element's center, as specified by the microrotation vector. Furthermore, to the rigid body movement of the overall volume element, the particles rotate locally. The laws of classical continuum mechanics are supplemented in the micropolar fluid concept with extra equations that account for the conservation of micro-inertia moments and the balance of first stress moments that arise when the microstructure of a material is taken into account, as well as additional local constitutive parameters [21]. Actually, micropolar liquids can be defined as the non-Newtonian liquids containing short rigid cylindrical elements or dumb-bell molecules, polymer fluids, animal blood, fluid suspensions, etc. Micropolar fluid dynamics can also be used to represent the presence of dust or smoke, especially in a gas [22].

Rotational flux is significant due to its implementation in science, engineering, and manufacturing industries. For foundation and modeling capabilities, various manufacturing objects rely on rotating flow's physics such as whirlpools, tornadoes, vacuum pumps, jet engines, tropical cyclones, centrifugal pumps, etc., since the phenomena of rotational flux are complex and analysts are trying comprehend the underlying science. Abbasi et al. [23] estimated the activation energy attributes and thermal radiation in axisymmetric revolving stagnation point flux of hybrid nanoliquid. Bilal et al. [24] illustrated the hall current impact on time-dependent carbon nanotubes rotational flux with dust particles and nonlinearly thermal radiation in a porous medium. Ali et al. [25] investigated the time-dependent rotating flux of a fractional Maxwell liquid in a cylinder subject to shear stress on the boundary. Donghwan Kim et al. [26] deliberated the operating parameters' impacts on in-cylindrical flux features of an optical accessible engine in the presence of a spray-guided injector. Liu et al. [27] studied the rotational flux dynamics in the friction stir welding of aluminum alloys.

Dust consists of solid dry particles of matter that is found in the air; the less viscous fluid incorporated in the solid dust particles is called dusty fluid. The formulation of rain drops because of little solid dust particles is a typical illustration of dusty air [28]. It was pointed out by Fortov et al. [29] that there exists equality between the force exerted on the gas by the dust and force exerted on the dust by the gas. Bilal et al. [30] studied the viscoelastic fluid subject to dust particles; Jalil et al. [31] examined the exact solution of the boundary value fluid problem; Reena and Rana [32] considered the micropolar fluid subject to solid dust particles; Dasman et al. [33] analyzed the non-Newtonian fluid incorporation of dust particles. More work on dusty fluid subject to various types of geometries was carried out in [34–38].

By studying the above-mentioned literature, we concluded that research work on the two-phase dusty micropolar fluid subject to Coriolis and Lorentz forces has not yet been performed. Motivated by the aforementioned wide scope of non-Newtonian fluid and dusty fluid applications, we decided to evaluate the currently elaborated dusty fluid problem. The primary purpose of the present investigation was to analyze the outcomes of distinct

parameters and volume concentrations of dust particles on the dynamics of micropolar dusty fluid across a stretching sheet. Very recently, research on non-Newtonian fluids has fascinated young researchers due to large-scale applications in different industries. By using similarity modifications, the relevant nonlinear PDEs are converted into a system of ODEs. The graphical outcomes of velocity, temperature, the skin friction factor, and the Nusselt number were investigated based on different inputs of physical parameters.

2. Mathematical Formulation

Let us analyze a incompressible time-independent 3D rotating laminar flux of dusty micropolar fluid across a stretching sheet. The sheet is stretched in xy-plane and fluid placed along the z-axis. Fluid revolves with constant velocity Ω around the z-axis. The feature of Coriolis forces in the primary momentum and secondary momentum equations are $+2\Omega v_1 \& -2\Omega v_2$, respectively. Although the first body force is positive, the velocity of secondary flow is negative, which creates an overall negative impact on the fluid primary velocity. The apparent and intended are two observable two paths in a rotatory frame of reference. The case of the intended/true path produces a trajectory that is easily deformed by some fictitious force, known as the Coriolis force, which influence the apparent path. Both fluid and dust particles were considered to be static at first. Dust particles are assumed to be evenly sized spheres with constant density all over the stream. Further, T_∞ and T_w are the liquid's ambient temperature and superficial temperature, respectively. Figure 1 displays the flux attributes and the coordinate system. For dusty phase flux, the model based on boundary layer approximation and physical assumptions and coupled with constraints is as follows [39–41].

$$\frac{\partial v_1}{\partial x} + \frac{\partial v_2}{\partial y} + \frac{\partial v_3}{\partial z} = 0, \tag{1}$$

$$(1-\phi_d)\left(v_1\frac{\partial v_1}{\partial x} + v_2\frac{\partial v_1}{\partial y} + v_3\frac{\partial v_1}{\partial z} - 2\Omega v_2\right) = (1-\phi_d)\left(\nu + \frac{k}{\rho}\right)\frac{\partial^2 v_1}{\partial z^2} + \frac{k}{\rho}\frac{\partial N_o}{\partial z} + \frac{KN}{\rho}(v_{1p} - v_1), \tag{2}$$

$$(1-\phi_d)\left(v_1\frac{\partial v_2}{\partial x} + v_2\frac{\partial v_2}{\partial y} + v_3\frac{\partial v_2}{\partial z} + 2\Omega v_1\right) = (1-\phi_d)\left(\nu + \frac{k}{\rho}\right)\frac{\partial^2 v_2}{\partial z^2} + \frac{KN}{\rho}(v_{2p} - v_2), \tag{3}$$

$$v_1\frac{\partial N_o}{\partial x} + v_2\frac{\partial N_o}{\partial y} + v_3\frac{\partial N_o}{\partial z} = \frac{\gamma}{\rho j}\frac{\partial^2 N_o}{\partial z^2} - \frac{k}{\rho j}\left(2N_o + \frac{\partial v_1}{\partial z}\right) \tag{4}$$

$$(\rho_{Cp})\left(v_1\frac{\partial T}{\partial x} + v_2\frac{\partial T}{\partial y} + v_3\frac{\partial T}{\partial z}\right) = k^*\left(\frac{\partial^2 T}{\partial z^2}\right) + \frac{\rho_p C_p}{\rho_{Cp}\tau_T}(T_p - T). \tag{5}$$

For dusty particle flow

$$\frac{\partial v_{1p}}{\partial x} + \frac{\partial v_{2p}}{\partial y} + \frac{\partial v_{3p}}{\partial z} = 0, \tag{6}$$

$$v_{1p}\frac{\partial v_{1p}}{\partial x} + v_{2p}\frac{\partial v_{1p}}{\partial y} + v_{3p}\frac{\partial v_{1p}}{\partial z} = 2\Omega v_{2p} + \frac{KN}{\rho}(v_1 - v_{1p}), \tag{7}$$

$$v_{1p}\frac{\partial v_{2p}}{\partial x} + v_{2p}\frac{\partial \hat{v_{2p}}}{\partial y} + v_{3p}\frac{\partial v_{2p}}{\partial z} + 2\Omega v_1 = \frac{KN}{\rho}(v_2 - v_{2p}), \tag{8}$$

$$v_1\frac{\partial T_p}{\partial x} + v_2\frac{\partial T_p}{\partial y} + v_3\frac{\partial T_p}{\partial z} = \frac{c_p}{c_m\tau_T}(T - T_p). \tag{9}$$

The relevant boundary conditions are [42–44]:

$$\left.\begin{aligned} v_1 = v_{1w} = ax, v_2 = 0, v_3 = 0,\ N_o = -\beta\frac{\partial v_1}{\partial z}, T = T_w,\ at\ z = 0, \\ v_{1p} = v_{1w} = ax, v_{2p} = 0, v_3 = 0,\ T_p = T_w,\ at\ z = 0, \\ v_1 \to 0, v_2 \to 0, v_3 \to v_3,\ N_o \to 0,\ T \to T_\infty,\ \ as\ z \to \infty, \\ v_{1p} \to 0, v_{2p} \to 0, v_{3p} \to v_3,\ T_p \to T_\infty,\ as\ z \to \infty, \end{aligned}\right\} \quad (10)$$

where, v_1, v_2, and v_3 are velocity components in x, y, and z direction, respectively. v_{1p}, v_{2p}, and v_{3p} denote the velocity of the components of dust particles; Ω represents angular velocity and N_o, a is a constant of stretching rate ($a > 0$); v_{1w} is stretching velocity component along the a-axis; N stands for micro-rotation and dust particle's number density. ν shows kinematic viscosity, K signifies the Stoke's drag constant, ρ deputizes the density of fluid, c_p delegates the specific heat capacity of fluid, k^* demonstrates the thermal conductivity, T symbolizes liquid's temperature, ρ_p signifies the density of dust particles, τ_T constitutes the thermal equilibrium time, C_p represents concentration of dust particles, c_m denotes the specific heat of dust particles, T_p is the temperature of the dust particle, j, k, and γ are micro-inertia per unit mass.

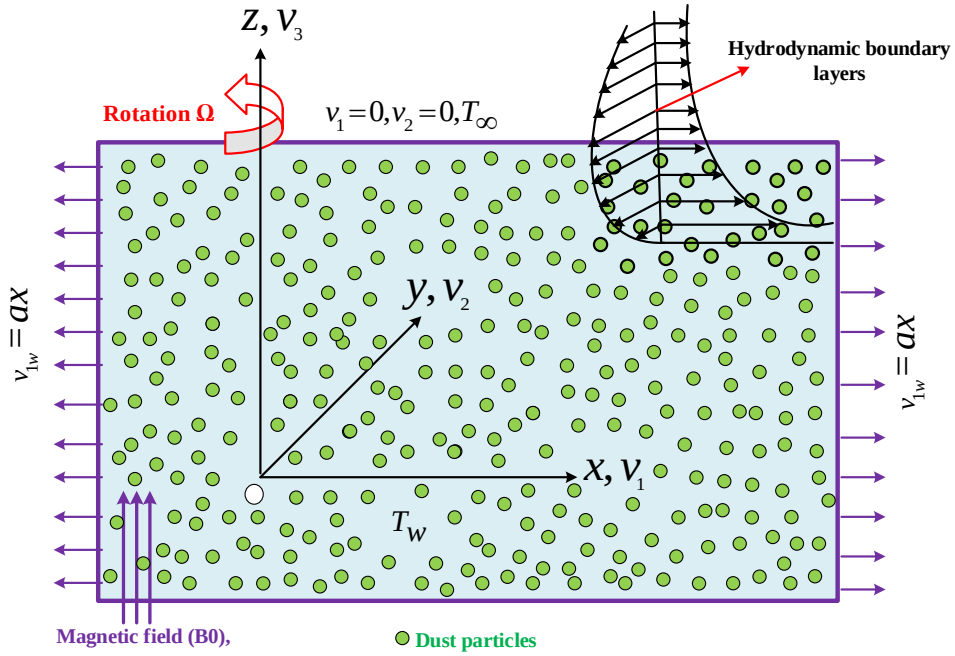

Figure 1. Schematic flow configuration.

The similarity transformation follows the work of [45,46]

$$\left.\begin{aligned} v_1 = axG_1'(\eta),\ v_2 = axG_2(\eta),\ v_3 = -\sqrt{a\nu}G_1(\eta),\ N_o = ax\sqrt{\frac{a}{\nu}}H(\eta),\ \eta = \left(\frac{a}{\nu}\right)^{\frac{1}{2}}z, \\ \theta(\eta) = \frac{T - T_\infty}{T_w - T_\infty}, \\ v_{1p} = axG_1'(\eta),\ v_{2p} = axG_2(\eta),\ v_{3p} = -\sqrt{a\nu}G_1(\eta),\ \eta = \sqrt{\frac{a}{\nu}}z \\ \theta_p(\eta) = \frac{T_p - T_\infty}{T_w - T_\infty}, \end{aligned}\right\} \quad (11)$$

where η denotes the similarity variable. Equation (1) is satisfied identically. By using transformations, Equations (2)–(9) have the following structure:

$$(1-\phi_d)(1+\Lambda)G_1''' + (1-\phi_d)(G_1G_1'' + 2RG_2 - G_1'^2) + \Lambda H' + \Gamma_v\gamma_v(G_{1p}' - G_1') = 0, \quad (12)$$

$$(1-\phi_d)(1+\Lambda)G_2'' + (1-\phi_d)(G_1G_2' - G_1'G_2 - 2RG_1') + \Gamma_v\gamma_v(G_{2p} - G_2) = 0, \quad (13)$$

$$(1+\frac{\Lambda}{2})H'' + G_1H' - G_1'H - (2H + G_1'') = 0 \quad (14)$$

$$\theta'' + Prf\theta' + Pr\gamma_t.\beta_t(\theta_p - \theta) = 0, \quad (15)$$

For the dusty phase

$$G_{1p}'^2 - G_{1p}G_{1p}'' - 2RG_{2p} + \gamma_v.\Gamma_v(G_{1p}' - G_1') = 0, \quad (16)$$

$$G_{1p}'G_{2p} - G_{1p}G_{2p}' + 2RG_{1p}' + \gamma_v.\Gamma_v(G_{2p} - G_2) = 0, \quad (17)$$

$$G_{1p}\theta_p' + \gamma_t.\beta_t(\theta - \theta_p) = 0, \quad (18)$$

with boundary constraints,

$$\left.\begin{aligned} G_1(\eta) = 0,\ G_2(\eta) = 0,\ G_1'(\eta) = 1, H = -\beta F_1'',\ \theta(\eta) = 1,\ at\ \eta = 0, \\ G_{1p}(\eta) = G_1(\eta),\ G_{2p}(\eta) = G_2(\eta),\ G_{1p}'(\eta) = 1, \theta_p(\eta) = 1,\ at\ \eta = 0, \\ G_1'(\eta) \to 0, G_2'(\eta) \to 0,\ \theta(\eta) \to 0,\ H = 0,\ at\ \eta \to \infty. \\ G_{1p}'(\eta) \to 0, G_{2p}'(\eta) \to 0,\ \theta_p(\eta) \to 0,\ at\ \eta \to \infty. \end{aligned}\right\} \quad (19)$$

where $Pr = \frac{\mu_f(cp)_f}{k_f}$ shows the Prandtl number, $\Lambda = \frac{k}{\mu}$ is the material parameter, $R = \frac{\Omega}{a}$ represents the rotational parameter, $\Gamma_v = \frac{1}{\tau_v c}$ denotes the fluid–particle interaction parameter for velocity, $\gamma_v = \frac{Nm}{\rho}$ is the mass concentration of dusty granules, $\gamma_t = \frac{c_p}{c_m}$ is the ratio of specific heat, and $\beta_t = \frac{1}{a\tau_T}$ is the fluid interaction parameter for temperature. This report is based upon the influence of volume fraction of dust particles subject to a small amount of dust $\phi_d = 0.2$ and a large amount of dust particles $\phi_d = 0.8$ when Coriolis and Lorentz forces are significant in the case of non-Newtonian fluid (micropolar fluid).

3. Physical Quantities

The important physical quantities of interest are discussed in this section. The Nusselt coefficients Nu_x and skin friction coefficients are given as [41,47]:

$$\left.\begin{aligned} Cf_x = \frac{\tau_{xz}}{\rho(ax)^2} \\ Cf_y = \frac{\tau_{yz}}{\rho(ax)^2} \\ Nu = \frac{xq_w}{k_f(T - T_\infty)} \end{aligned}\right\} \quad (20)$$

with

$$q_w = -k\frac{\partial T}{\partial z}|_{z=0} ..., j_w = -D\frac{\partial C}{\partial z}|_{z=0} \quad (21)$$

Finally we have,

$$\left.\begin{aligned} (Re_x)^{0.5}Cf_x = (1+\Lambda)G_1''(0) \\ (Re_x)^{0.5}Cf_y = (1+\Lambda)G_2'(0) \\ (Re_x)^{-0.5}Nu = -\theta'(0) \end{aligned}\right\} \quad (22)$$

$Re_x = \frac{u_w^2}{cv}$ stands for local Reynolds number.

4. Solution Procedure

A system of ordinary differential equations represents the flow model. The Equations (11)–(16) are numerically solved using the effectiveness and strength of numerical computing in the bvp4c approach using MATLAB. Ref. [48] provides more details on this solution approach (see Figure 2). The graphical and numerical results show the velocity and temperature fields as different physical factors. The bvp4c technique is used to transform the system of ODEs (11)–(16) into first-order ODEs for a solution:

$$\lambda_1' = \lambda_2,$$
$$\lambda_2' = \lambda_3,$$
$$\lambda_3' = \frac{(-1)}{(1-\phi_d)(1+\Lambda)}[(1-\phi_d)(\lambda_1\lambda_3 + 2R\lambda_4 - \lambda^2) + \Lambda\lambda_6 + \Gamma_v\gamma_v(\lambda_{11} - \lambda_2)],$$
$$\lambda_4' = \lambda_5,$$
$$\lambda_5' = \frac{(-1)}{(1-\phi_d)(1+\Lambda)}[(1-\phi_d)(\lambda_1\lambda_5 - \lambda_2\lambda_4 - 2R\lambda_2) + \Gamma_v\gamma_v(\lambda_{12} - \lambda_4)],$$
$$\lambda_6' = \lambda_7,$$
$$\lambda_7' = \frac{(-1)}{\left(1+\frac{\Lambda}{2}\right)}[\lambda_1\lambda_7 - \lambda_2\lambda_6 - (2\lambda_6 + \lambda_3)],$$
$$\lambda_8' = \lambda_9$$
$$\lambda_9' = (-1)[\lambda_9\lambda_1 + Pr\Gamma_t\beta_t(\lambda_{14} - \lambda_8)],$$
$$\lambda_{11}' = \frac{(1)}{\lambda_{10}}[\lambda_{11}^2 - 2R\lambda_{12} + \Gamma_v\gamma_v(\lambda_{11} - \lambda_2)],$$
$$\lambda_{12}' = \frac{(1)}{\lambda_{10}}[\lambda_{11}\lambda_{12} + 2R\lambda_{11} + \Gamma_v\gamma_v(\lambda_{12} - \lambda_4)],$$
$$\lambda_{13}' = \frac{(-1)}{\lambda_{10}}[\beta_t\gamma_t(\lambda_8 - \lambda_{13})].$$

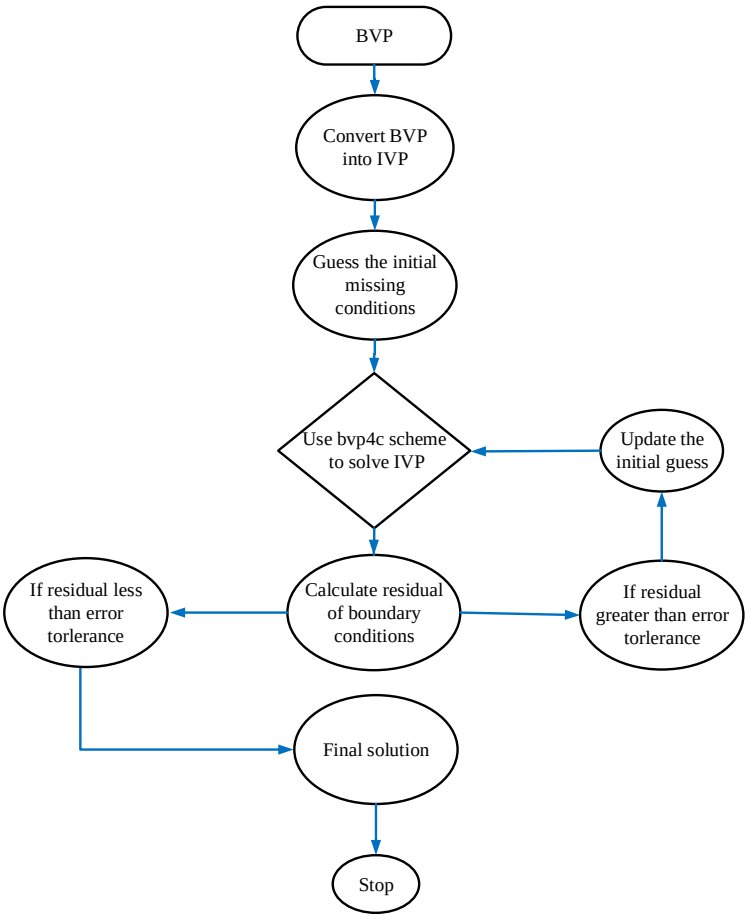

Figure 2. Numerical solution flow chart.

The corresponding boundary conditions are as follows:
$\lambda_1 = 0,\ \lambda_2 = 1,\ \lambda_4 = 0,\ \lambda_6 = -\beta\lambda_3,\ at\ \eta = 0,$
$\lambda_8 = 0,\ \lambda_9 = 1,\ \lambda_1 1 = 0,\ \lambda_{13} = 1,\ at\ \eta = 0,$
$\lambda_2 \to 0,\ \lambda_5 \to 0,\ \lambda_6 \to 0,\ as\ \eta \to \infty.$
$\lambda_9 \to 0,\ \lambda_{12} \to 0,\ \lambda_{13} \to 0,\ as\ \eta \to \infty.$

5. Results and Discussion

The main purpose of this investigation is to analyze the thermal transportation and flux of the micropolar fluid on a stretching surface with a suspension of dust particles. For solving highly nonlinear equations with related constraint, the bvp4c approach is applied and coded in MATLAB; graphical outcomes of the impacts of the variational behavior of different parameters on velocity and temperature and a micro-rotation distribution profile for both fluid and dusty phases were acquired. The outcomes for Nusselt number, skin friction factor, and couple stress were obtained graphically. Before plotting the results, we have justified our results with the already published research articles through Tables 1 and 2 subject to limited cases. An excellent correlation has been achieved which affirms the validity of numerical technique coded in MATLAB. The values of parameters that we used are as follows: $R = 0.5$, $Pr = 0.72$, $\phi_d = 0.1$ and 0.8, $\Gamma_v = 1$, $\beta_t = 0.1$, $\gamma_v = 0.2$, $\gamma_t = 0.2$, $\Lambda = 0.2$, and $\beta = 0.5$.

Table 1. Comparing the current numerical findings for M when and all others parameter are zero.

M	Rehman [49]	Bagh [50]	Present Results
0.0	1.00000130	1.0000080	1.000013
0.2	1.0954463	1.0954458	1.095446
0.5	1.2247454	1.2247446	1.224745
1.0	1.4142180	1.4142132	1.414218

Table 2. Comparing the current numerical findings for Pr when and all others parameter are zero.

Pr	Rehman [49]	Bagh [50]	Present Results
1.0	1.00000	1.0000	1.0000
3.0	1.92375	1.9236	1.9238
10.0	3.72061	3.7207	3.7210
100.0	12.29404	12.2940	1.2941

Figure 3a,b depicts the impact of rotating and dust particle volume concentration on axial and transverse velocity of fluid. It reveals that there is deceleration in G_1' with amplifying inputs of R and ϕ_d. This velocity acquires its maximum value in condition of $R = 0$ (pure stretching case). As a result of Coriolis forces, the motion of the fluid slows down; the transverse velocity G_2 has the opposite behavior, with incremented values of R and ϕ_d. Similarly, by increasing dust particle concentration, the fluid becomes thicker and offers resistance to motion, so G_1' reduced. Figure 4a,b demonstrate the influence of R and ϕ_d on the velocities of the dusty phase of fluid. Here, G_{1p} and G_{2p} signifies the momentum boundary layers for dusty phase in x and y direction, respectively. The axial velocity of the dusty phase of fluid recedes due to the growing strength of both dust particle concentration and rotating parameter; however, transverse velocity increases against these parameters. Figure 5a,b are plotted to see the effect of the material parameter and ϕ_d on G_1' and G_2. The axial velocities increased with amplified values of material parameter; however, transverse velocity decreased. Since the material parameter Λ is inversely proportional to the dynamic viscosity coefficients, its higher value indicates a reduction in viscous impacts, allowing the flow to move faster; for higher inputs of ϕ_d, both velocities are decreased.

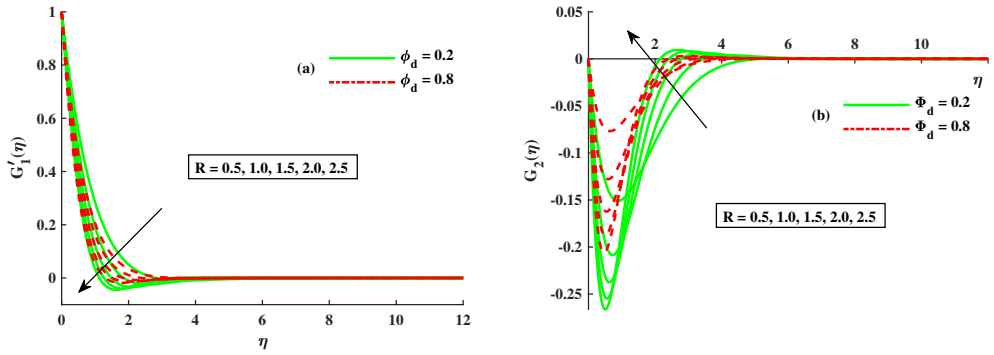

Figure 3. Fluctuation of R and ϕ_d on $G_1'(\eta)$ and $G_2(\eta)$.

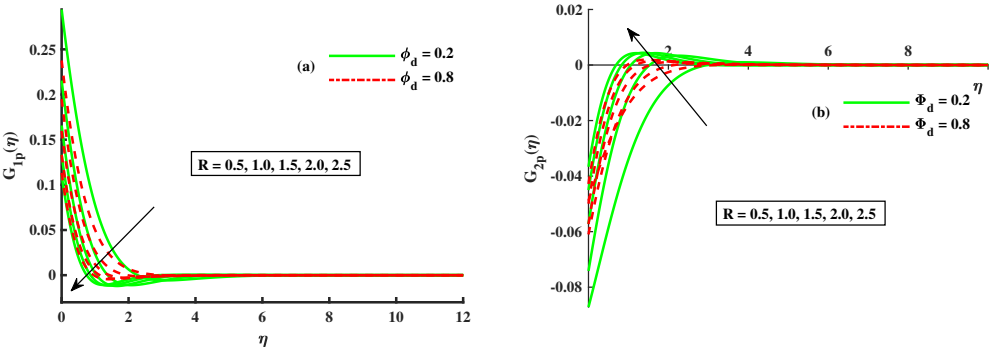

Figure 4. Fluctuation of R and ϕ_d on $G_{1p}(\eta)$ and $G_{2p}(\eta)$.

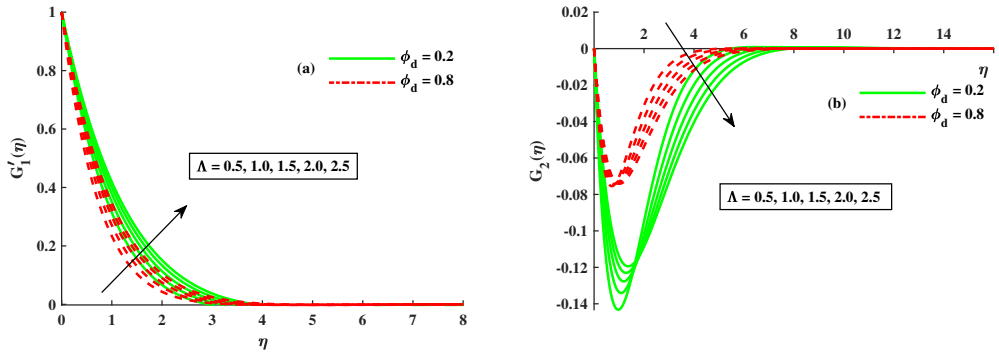

Figure 5. Fluctuation of Λ and ϕ_d on $G_1'(\eta)$ and $G_2(\eta)$.

Figure 6a,b demonstrate the affect of Λ and volume concentration of dust particles on dusty phase velocities G_{1p} and G_{2p}. It can be seen that G_{1p} velocity increased and G_{2p} velocity decreased with incremental values of material parameters; both velocities decreased with higher inputs of dust particle concentration. Figure 7a,b display the variation in micro-rotation distribution profile with varying inputs of rotational, material parameter, and concentration of dust particles. From Figure 7a, we can see that the micro-rotation profile was amplified with larger inputs of R, whereas it was reduced against higher inputs of dust particle concentration. Figure 7b reveals that micro-rotation was improved with increasing inputs of Λ parameters. Figure 8a,b illustrate the impact of R and ϕ_d on the temperature and dust phase of the fluid. It is obvious that the temperature of fluid and dusty phase increased with increasing inputs of R and ϕ_d. Basically, the development of heat is satisfied on the base of a higher diffusion process because of increased rotation. Figure 9a,b represent the fluctuation in θ and θ_p by different values of the material parameter and ϕ_d. The fluid temperature and dust phase temperature depreciate against magnified inputs of the material parameter; both phase temperatures rise with larger inputs of ϕ_d. Physically, the higher input of dust particles enhance the base fluid dust concentration, which causes the fluid velocity to decrease; however, the base fluid temperature increased due to the thermal conductivity of the additional dust particles.

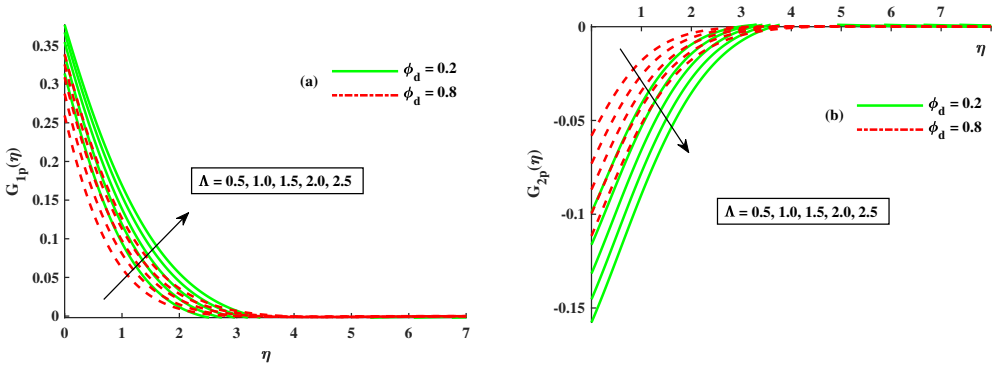

Figure 6. Fluctuation of Λ and ϕ_d on G_{1p} and G_{2p}.

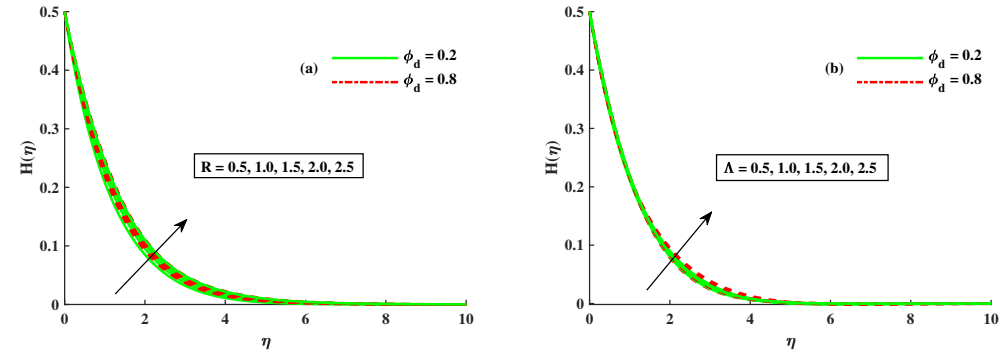

Figure 7. Fluctuation of R, Λ and ϕ_d on $H(\eta)$.

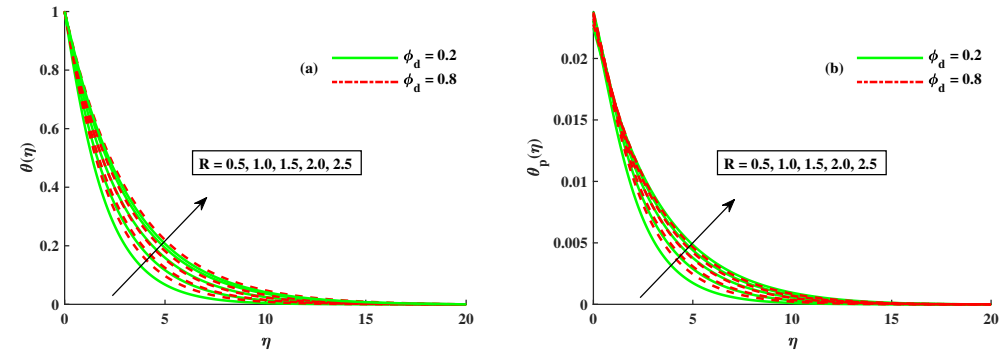

Figure 8. Fluctuation of R and ϕ_d on θ and θ_p.

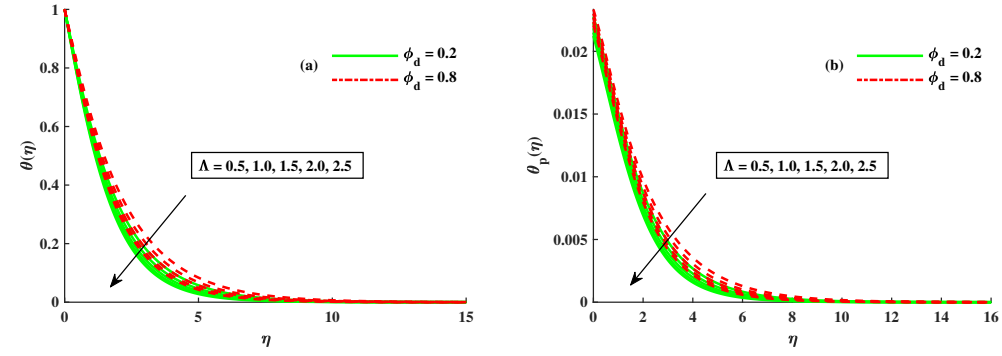

Figure 9. Fluctuation of Λ and ϕ_d on θ and θ_p.

Figure 10a,b portray the skin friction factor in x and y direction for different inputs of rotating parameter, material parameter, and dust particle concentration parameter. Figure 10a shows that the skin friction coefficient Cf_x was reduced against the enhanced values of Λ, R, and ϕ_d. Figure 10b reveals that the skin friction coefficient Cf_y depreciated against increasing values of the rotating parameter corresponding to the strong Coriolis

force in the rotating system, but displayed the opposite behavior against Λ and ϕ_d. The larger strength of the rotating parameter generated the instability in the fluid flow, and this oscillation characteristic is reduced when low values of R are considered. We can infer that a critical rotating condition exists for which secondary flow is sustainable, and all the while, the fluid primary flow is stable. The excessive velocity of the rotational fluid system is not useful, and considering this, a reasonable choice of Ω is recommended for functional producing activities. The influence of different parameters on the Nusselt number are sketched in Figure 11a. From Figure 11a, we see that the Nusselt number reduced with rising values of rotation, material parameter, and volume concentration of dust particles. Figure 11b depicts the fluctuation of couple stress by rotation, material parameter, and volume concentration of dust particles. It displays an increasing behavior against the rising values of all parameters. The large values of R cause the fluid primary velocity to slow down, which is responsible for increasing the fluid temperature; a low Nusselt number implies a higher temperature.

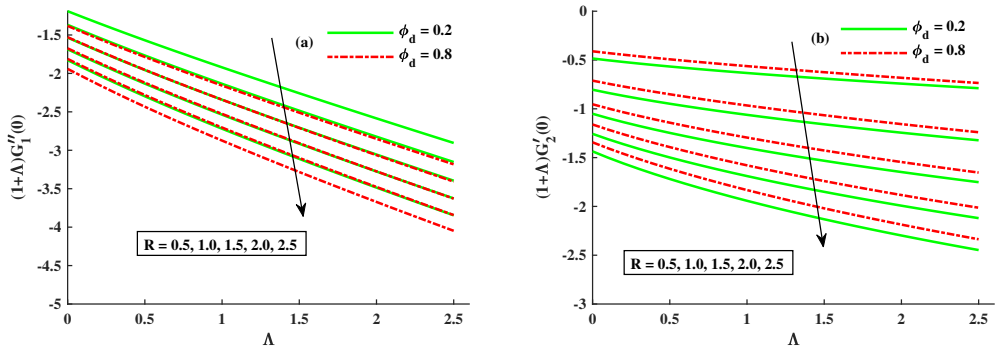

Figure 10. Fluctuation of R, Λ, and ϕ_d on $G_1''(0)$ and $G_2'(0)$.

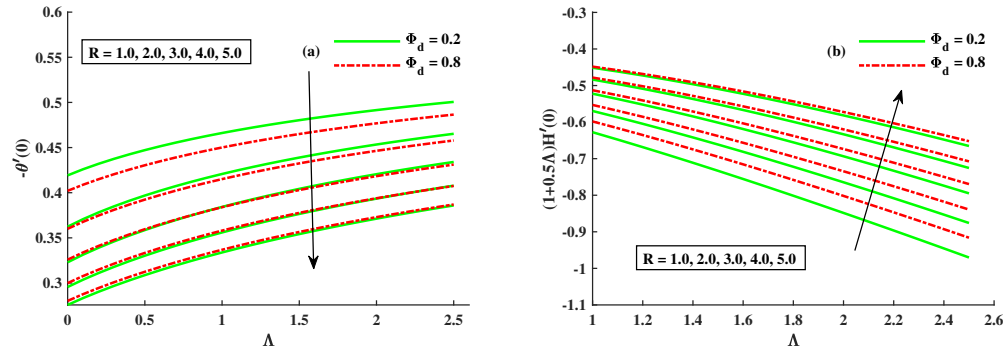

Figure 11. Fluctuation of R, Λ, and ϕ_d on Nusselt number and couple stress.

6. Conclusions

Efforts have been made to analyze the significance of micropolar dusty fluid and heat flux due to thermal boundary gradients across a stretching sheet. The non-dimensional problem is solved by using the bvp4c method developed in MATLAB script. Based on the consequences, it is reasonable to conclude that:

- $G_1'(\eta)$ and $G_{1p}(\eta)$ significantly decrease along with rising values of parameters ϕ_d, R and having increasing behavior against Λ, whereas $G_2(\eta)$ and $G_{2p}(\eta)$ have the opposite behavior against ϕ_d, R parameters while it decreased against Λ.
- The micro-rotation distribution profile depreciates by higher inputs of ϕ_d and amplified with larger inputs of rotation and material parameter.
- The temperature θ and θ_p aggrandize with higher inputs of volume concentration of dust particles and rotation parameter, whereas it declines against increasing inputs of Λ.
- Along the x direction, the coefficient of skin friction decreased with enhancing values of Λ, ϕ_d, and R. Along the y-direction, the skin friction coefficient is raised by enlarge-

ment in Λ and ϕ_d, but it has opposite behavior against increasing inputs of rotating parameter.
- The magnitude of the Nusselt number is reduced with a higher contribution of R, ϕ_d, and Λ, whereas couple stress exhibit rising behavior against these parameters.

Through this successful numerical computational effort, we have successfully elucidated the parametric impacts on the dynamics of micropolar dusty fluid. This study may be extended for Maxwell dusty nanofluid, Oldroyd-B dusty nanofluid, and viscoelastic Jeffrey's dusty nanofluid.

Author Contributions: Q.L. modeled the problem and wrote the manuscript. B.A. completed the formal analysis and revision. S.U.R. and D.H. thoroughly checked the mathematical modeling, English corrections, formal analysis, and revision. S.A. solved the problem using MATLAB software. N.A.S. and J.D.C.: writing—review and editing. All authors finalized the manuscript after its internal evaluation. Q.L. and N.A.S. contributed equally to this work and are co-first authors. All authors have read and agreed to the published version of the manuscript.

Funding: This work was supported by the Korean Institute of Energy Technology Evaluation and Planning (KETEP) grant funded by the Korean government (MOTIE) (No. 20192010107020, Development of hybrid adsorption chiller using unutilized heat source of low temperature).

Institutional Review Board Statement: Not applicable.

Informed Consent Statement: Not applicable.

Data Availability Statement: Not applicable.

Conflicts of Interest: The authors declare no conflict of interest.

References

1. Eringen, A.C. Theory of micropolar fluids. *J. Math. Mech.* **1966**, *16*, 1–18. [CrossRef]
2. Eringen, A.C. Theory of thermomicrofluids. *J. Math. Anal. Appl.* **1972**, *38*, 480–496. [CrossRef]
3. Ariman, T.; Turk, M.; Sylvester, N. Microcontinuum fluid mechanics—A review. *Int. J. Eng. Sci.* **1973**, *11*, 905–930. [CrossRef]
4. Ariman, T.; Turk, M.; Sylvester, N. Applications of microcontinuum fluid mechanics. *Int. J. Eng. Sci.* **1974**, *12*, 273–293. [CrossRef]
5. Peddieson, J. Boundary layer theory for a micropolar fluid. *Recent Adv. Eng. Sci.* **1970**, *5*, 405–426.
6. Lukaszewicz, G. *Micropolar Fluids: Theory and Application*; Birkhäuser: Boston, MA, USA, 1999.
7. Eringen, A.C. *Microcontinuum Field Theories: II. Fluent Media*; Springer Science & Business Media: New York, NY, USA, 2001; Volume 2.
8. Xia, W.F.; Animasaun, I.; Wakif, A.; Shah, N.A.; Yook, S.J. Gear-generalized differential quadrature analysis of oscillatory convective Taylor-Couette flows of second-grade fluids subject to Lorentz and Darcy-Forchheimer quadratic drag forces. *Int. Commun. Heat Mass Transf.* **2021**, *126*, 105395. [CrossRef]
9. Dawar, A.; Wakif, A.; Thumma, T.; Shah, N.A. Towards a new MHD non-homogeneous convective nanofluid flow model for simulating a rotating inclined thin layer of sodium alginate-based Iron oxide exposed to incident solar energy. *Int. Commun. Heat Mass Transf.* **2022**, *130*, 105800. [CrossRef]
10. Yu, C.J.; Richter, A.; Datta, A.; Durbin, M.; Dutta, P. Observation of molecular layering in thin liquid films using X-ray reflectivity. *Phys. Rev. Lett.* **1999**, *82*, 2326. [CrossRef]
11. Kim, S.H.; Choi, S.R.; Kim, D. Thermal conductivity of metal-oxide nanofluids: Particle size dependence and effect of laser irradiation. *J. Heat Transfer.* **2007**, *129*, 298–307. [CrossRef]
12. Prasannakumara, B.C.; Shashikumar, N.S.; Archana, M. Three-dimensional boundary layer flow and heat transfer of a dusty fluid towards a stretching sheet with convective boundary conditions. *J. Comput. Appl. Res. Mech. Eng.* **2018**, *8*, 25–38.
13. Ali, L.; Ali, B.; Liu, X.; Iqbal, T.; Zulqarnain, R.M.; Javid, M. A comparative study of unsteady MHD Falkner–Skan wedge flow for non-Newtonian nanofluids considering thermal radiation and activation energy. *Chin. J. Phys.* **2022**, *77*, 1625–1638. [CrossRef]
14. Wang, F.; Asjad, M.I.; Ur Rehman, S.; Ali, B.; Hussain, S.; Gia, T.N.; Muhammad, T. MHD Williamson Nanofluid Flow over a Slender Elastic Sheet of Irregular Thickness in the Presence of Bioconvection. *Nanomaterials* **2021**, *11*, 2297. [CrossRef] [PubMed]
15. Wang, F.; Rehman, S.; Bouslimi, J.; Khaliq, H.; Qureshi, M.I.; Kamran, M.; Alharbi, A.N.; Ahmad, H.; Farooq, A. Comparative study of heat and mass transfer of generalized MHD Oldroyd-B bio-nano fluid in a permeable medium with ramped conditions. *Sci. Rep.* **2021**, *11*, 23454. [CrossRef] [PubMed]
16. Fuzhang, W.; Akhtar, S.; Nadeem, S.; El-Shafay, A. Mathematical computations for the physiological flow of Casson fluid in a vertical elliptic duct with ciliated heated wavy walls. *Waves Random Complex Media* **2022**, *4*, 1–14. [CrossRef]
17. Anuar, N.S.; Bachok, N. Double solutions and stability analysis of micropolar hybrid nanofluid with thermal radiation impact on unsteady stagnation point flow. *Mathematics* **2021**, *9*, 276. [CrossRef]

18. Ali, L.; Ali, B.; Abd Allah, A.M.; Hammouch, Z.; Hussain, S.; Siddique, I.; Huang, Y. Insight into significance of thermal stratification and radiation on dynamics of micropolar water based TiO_2 nanoparticle via finite element simulation. *J. Mater. Res. Technol.* **2022**, *19*, 4209–4219. [CrossRef]
19. Wang, W.; Jaradat, M.M.; Siddique, I.; Mousa, A.A.A.; Abdal, S.; Mustafa, Z.; Ali, H.M. On Thermal Distribution for Darcy–Forchheimer Flow of Maxwell Sutterby Nanofluids over a Radiated Extending Surface. *Nanomaterials* **2022**, *12*, 1834. [CrossRef]
20. Ali, L.; Liu, X.; Ali, B.; Mujeed, S.; Abdal, S.; Mutahir, A. The impact of nanoparticles due to applied magnetic dipole in micropolar fluid flow using the finite element method. *Symmetry* **2020**, *12*, 520. [CrossRef]
21. Nabwey, H.A.; Rashad, A.M.; Mahdy, A.E.N.; Shaaban, S.M. Thermal Conductivity and Thermophoretic Impacts of Micropolar Fluid Flow by a Horizontal Absorbent Isothermal Porous Wall with Heat Source/Sink. *Mathematics* **2022**, *10*, 1514. [CrossRef]
22. Ghadikolaei, S.; Hosseinzadeh, K.; Hatami, M.; Ganji, D. MHD boundary layer analysis for micropolar dusty fluid containing Hybrid nanoparticles (Cu-Al2O3) over a porous medium. *J. Mol. Liq.* **2018**, *268*, 813–823. [CrossRef]
23. Abbasi, A.; Gulzar, S.; Mabood, F.; Farooq, W. Nonlinear thermal radiation and activation energy features in axisymmetric rotational stagnation point flow of hybrid nanofluid. *Int. Commun. Heat Mass Transf.* **2021**, *126*, 105335. [CrossRef]
24. Bilal, M.; Ramzan, M. Hall current effect on unsteady rotational flow of carbon nanotubes with dust particles and nonlinear thermal radiation in Darcy–Forchheimer porous media. *J. Therm. Anal. Calorim.* **2019**, *138*, 3127–3137. [CrossRef]
25. Ali Zafar, A.; Bilal Riaz, M.; Imran Asjad, M. Unsteady rotational flow of fractional Maxwell fluid in a cylinder subject to shear stress on the boundary. *Punjab Univ. J. Math.* **2020**, *50*, 21–32.
26. Kim, D.; Son, Y.; Park, S. Effects of operating parameters on in-cylinder flow characteristics of an optically accessible engine with a spray-guided injector. *Energy* **2022**, *245*, 123314. [CrossRef]
27. Liu, X.; Sun, Y.; Morisada, Y.; Fujii, H. Dynamics of rotational flow in friction stir welding of aluminium alloys. *J. Mater. Process. Technol.* **2018**, *252*, 643–651. [CrossRef]
28. Koriko, O.K.; Adegbie, K.S.; Shah, N.A.; Animasaun, I.L.; Olotu, M.A. Numerical solutions of the partial differential equations for investigating the significance of partial slip due to lateral velocity and viscous dissipation: The case of blood-gold Carreau nanofluid and dusty fluid. *Numer. Methods Part. Differ. Equ.* **2021**, *7*, 1–15. [CrossRef]
29. Fortov, V.; Vaulina, O.; Petrov, O.; Vasiliev, M.; Gavrikov, A.; Shakova, I.; Vorona, N.; Khrustalyov, Y.V.; Manohin, A.; Chernyshev, A. Experimental study of the heat transport processes in dusty plasma fluid. *Phys. Rev. E* **2007**, *75*, 026403. [CrossRef] [PubMed]
30. Bilal, M.; Khan, S.; Ali, F.; Arif, M.; Khan, I.; Nisar, K.S. Couette flow of viscoelastic dusty fluid in a rotating frame along with the heat transfer. *Sci. Rep.* **2021**, *11*, 1–16. [CrossRef]
31. Jalil, M.; Asghar, S.; Yasmeen, S. An exact solution of MHD boundary layer flow of dusty fluid over a stretching surface. *Math. Probl. Eng.* **2017**, *2017*, 1–5. [CrossRef]
32. Reena, R.; Rana, U. Effect of dust particles on rotating micropolar fluid heated from below saturating a porous medium. *Appl. Appl. Math. Int. J.* **2009**, *4*, 15.
33. Dasman, A.; Arifin, N.S.; Kasim, A.R.M.; Yacob, N.A. Formulation of dusty micropolar fluid mathematical model. *J. Phys. Conf. Ser.* **2019**, *1366*, 012032. [CrossRef]
34. Ramzan, M.; Shaheen, N.; Chung, J.D.; Kadry, S.; Chu, Y.M.; Howari, F. Impact of Newtonian heating and Fourier and Fick's laws on a magnetohydrodynamic dusty Casson nanofluid flow with variable heat source/sink over a stretching cylinder. *Sci. Rep.* **2021**, *11*, 2357. [CrossRef]
35. Ghadikolaei, S.; Hosseinzadeh, K.; Yassari, M.; Sadeghi, H.; Ganji, D. Boundary layer analysis of micropolar dusty fluid with TiO2 nanoparticles in a porous medium under the effect of magnetic field and thermal radiation over a stretching sheet. *J. Mol. Liq.* **2017**, *244*, 374–389. [CrossRef]
36. Varun Kumar, R.; Punith Gowda, R.; Naveen Kumar, R.; Radhika, M.; Prasannakumara, B. Two-phase flow of dusty fluid with suspended hybrid nanoparticles over a stretching cylinder with modified Fourier heat flux. *SN Appl. Sci.* **2021**, *3*, 384. [CrossRef]
37. Arifin, N.S.; Kasim, A.R.M.; Zokri, S.M.; Salleh, M.Z. Boundary Layer Flow of Dusty Williamson Fluid with Variable Viscosity Effect Over a Stretching Sheet. *J. Adv. Res. Fluid Mech. Therm. Sci.* **2021**, *86*, 164–175. [CrossRef]
38. Wang, F.; Khan, S.A.; Gouadria, S.; El-Zahar, E.R.; Khan, M.I.; Khan, S.U.; Yasir, M.; Li, Y.M. Entropy optimized flow of Darcy-Forchheimer viscous fluid with cubic autocatalysis chemical reactions. *Int. J. Hydrogen Energy* **2022**, *47*, 13911–13920. [CrossRef]
39. Rashid, S.; Hayat, T.; Qayyum, S.; Ayub, M.; Alsaedi, A. Three-dimensional rotating Darcy–Forchheimer flow with activation energy. *Int. J. Numer. Methods Heat Fluid Flow* **2019**, *29*, 935–948. [CrossRef]
40. Tayyab, M.; Siddique, I.; Jarad, F.; Ashraf, M.K.; Ali, B. Numerical solution of 3D rotating nanofluid flow subject to Darcy-Forchheimer law, bio-convection and activation energy. *S. Afr. J. Chem. Eng.* **2022**, *40*, 48–56. [CrossRef]
41. Ahmad, K.; Nazar, R.; Ishak, A.; Pop, I. Unsteady three-dimensional boundary layer flow due to a stretching surface in a micropolar fluid. *Int. J. Numer. Methods Fluids* **2012**, *68*, 1561–1573. [CrossRef]
42. Abbas, Z.; Javed, T.; Sajid, M.; Ali, N. Unsteady MHD flow and heat transfer on a stretching sheet in a rotating fluid. *J. Taiwan Inst. Chem. Eng.* **2010**, *41*, 644–650. [CrossRef]
43. Thumma, T.; Wakif, A.; Animasaun, I.L. Generalized differential quadrature analysis of unsteady three-dimensional MHD radiating dissipative Casson fluid conveying tiny particles. *Heat Transf.* **2020**, *49*, 2595–2626. [CrossRef]
44. Manghat, R.; Siddabasappa, S. MHD Boundary Layer Flow and Heat Transfer of Rotating Dusty Nanofluid over a Stretching Surface. *Kyungpook Math. J.* **2020**, *60*, 853–867.

45. Muhammad, S.; Ali, G.; Shah, Z.; Islam, S.; Hussain, S.A. The rotating flow of magneto hydrodynamic carbon nanotubes over a stretching sheet with the impact of non-linear thermal radiation and heat generation/absorption. *Appl. Sci.* **2018**, *8*, 482. [CrossRef]
46. Awan, A.U.; Ahammad, N.A.; Majeed, S.; Gamaoun, F.; Ali, B. Significance of hybrid nanoparticles, Lorentz and Coriolis forces on the dynamics of water based flow. *Int. Commun. Heat Mass Transf.* **2022**, *135*, 106084. [CrossRef]
47. Oyelakin, I.; Lalramneihmawii, P.; Mondal, S.; Sibanda, P. Analysis of double-diffusion convection on three-dimensional MHD stagnation point flow of a tangent hyperbolic Casson nanofluid. *Int. J. Ambient Energy* **2020**, *7*, 1–12. [CrossRef]
48. Habib, U.; Abdal, S.; Siddique, I.; Ali, R. A comparative study on micropolar, Williamson, Maxwell nanofluids flow due to a stretching surface in the presence of bioconvection, double diffusion and activation energy. *Int. Commun. Heat Mass Transf.* **2021**, *127*, 105551. [CrossRef]
49. Rehman, S.U.; Mariam, A.; Ullah, A.; Asjad, M.I.; Bajuri, M.Y.; Pansera, B.A.; Ahmadian, A. Numerical computation of buoyancy and radiation effects on MHD micropolar nanofluid flow over a stretching/shrinking sheet with heat source. *Case Stud. Therm. Eng.* **2021**, *25*, 100867. [CrossRef]
50. Ali, B.; Nie, Y.; Khan, S.A.; Sadiq, M.T.; Tariq, M. Finite element simulation of multiple slip effects on MHD unsteady maxwell nanofluid flow over a permeable stretching sheet with radiation and thermo-diffusion in the presence of chemical reaction. *Processes* **2019**, *7*, 628. [CrossRef]